



Article

Complementary, Cooperative Ditopic Halogen Bonding and Electron Donor-Acceptor π - π Complexation in the Formation of Cocrystals

Erin D. Speetzen ¹, Chideraa I. Nwachukwu ², Nathan P. Bowling ¹  and Eric Bosch ^{2,*} 

¹ Department of Chemistry, University of Wisconsin-Stevens Point, 2101 South Avenue, Stevens Point, WI 54481, USA; espeetze@uwsp.edu (E.D.S.); nbowling@uwsp.edu (N.P.B.)

² Chemistry Department, Missouri State University, 901 South National Avenue, Springfield, MO 65897, USA; nwachukwu123@live.missouristate.edu

* Correspondence: ericbosch@missouristate.edu

Abstract: This study expands and combines concepts from two of our earlier studies. One study reported the complementary halogen bonding and π - π charge transfer complexation observed between isomeric electron rich 4-*N,N*-dimethylaminophenylethynylpyridines and the electron poor halogen bond donor, 1-(3,5-dinitrophenylethynyl)-2,3,5,6-tetrafluoro-4-iodobenzene while the second study elaborated the ditopic halogen bonding of activated pyrimidines. Leveraging our understanding on the combination of these non-covalent interactions, we describe cocrystallization featuring ditopic halogen bonding and π -stacking. Specifically, red cocrystals are formed between the ditopic electron poor halogen bond donor 1-(3,5-dinitrophenylethynyl)-2,4,6-trifluoro-3,5-diiodobenzene and each of electron rich pyrimidines 2- and 5-(4-*N,N*-dimethyl-aminophenylethynyl)pyrimidine. The X-ray single crystal structures of these cocrystals are described in terms of halogen bonding and electron donor-acceptor π -complexation. Computations confirm that the donor-acceptor π -stacking interactions are consistently stronger than the halogen bonding interactions and that there is cooperativity between π -stacking and halogen bonding in the crystals.

Keywords: ditopic halogen bonding; electron donor acceptor complexation; pi-stacking; cooperative halogen bonding and electron donor acceptor complexation; complementary halogen bonding and electron donor acceptor complexation; charge-transfer complexation; tetrel bonding



Citation: Speetzen, E.D.; Nwachukwu, C.I.; Bowling, N.P.; Bosch, E. Complementary, Cooperative Ditopic Halogen Bonding and Electron Donor-Acceptor π - π Complexation in the Formation of Cocrystals. *Molecules* **2022**, *27*, 1527. <https://doi.org/10.3390/molecules27051527>

Academic Editors:
Gotzone Barandika and Zhiwu Yu

Received: 27 December 2021

Accepted: 17 February 2022

Published: 24 February 2022

Publisher's Note: MDPI stays neutral with regard to jurisdictional claims in published maps and institutional affiliations.



Copyright: © 2022 by the authors. Licensee MDPI, Basel, Switzerland. This article is an open access article distributed under the terms and conditions of the Creative Commons Attribution (CC BY) license (<https://creativecommons.org/licenses/by/4.0/>).

1. Introduction

The cooperative interplay between non-covalent interactions is a current topic of interest [1,2]. Indeed, the deliberate preparation of supramolecular complexes, polymers and networks in the crystalline state relies on the intentional exploitation of multiple cooperative non-covalent interactions [3–7]. While it is reasonable to expect concomitant π -stacking in halogen bonded cocrystals formed between halobenzenes and pyridines the intentional coupling of halogen bonding and π -stacking is increasingly recognized as important in crystal engineering and supramolecular assembly. Halogen bonding and π -stacking have been incorporated as key cooperative non-covalent interactions in the [2+2] photoreaction in oocrystals including dipyrindylethylenes [8]. Cooperative halogen bonding and π -stacking also feature in the preparation of luminescent materials [9] and semiconductors [10] amongst other applications. Clearly, recognition and exploitation of charge-transfer in p-stacked interactions has potential in optoelectronics [11]. Earlier we described cocrystallization based on cooperative halogen bonding and electron donor-acceptor π -complexation to form colored cocrystals [12]. In that study, which forms the basis for the current report, two complimentary molecules were designed to each include a halogen bonding site and an enhanced electron donor-acceptor π -complexation as illustrated in Figure 1a. Thus, molecule A has a pyridyl moiety as halogen bond acceptor

along with an electron rich *N,N*-dimethylaminophenyl moiety for enhanced electron donor-acceptor (EDA) π -stacking. Complementary molecule B has an iodotetrafluorophenyl moiety as halogen bond donor and an electron poor dinitrophenyl moiety for complementary EDA π -stacking. Slow evaporation of an equimolar solution of A and B yielded a homogeneous mass of bright red crystals. The single crystal X-ray structure of the red crystals confirmed the formation of alternating -ABAB- π -stacked, halogen bonded, molecules. In a separate study we demonstrated that electron rich pyrimidines, related to molecule A, such as 5-(4-*N,N*-dimethylaminophenyl-ethynyl)pyrimidine, are viable ditopic halogen bond acceptors and form cocrystals with ditopic halogen bond donors such as 1,3-diiidotetrafluorobenzene. These cocrystals feature zig-zag one dimensional supramolecular polymers as shown in Figure 1b [13].

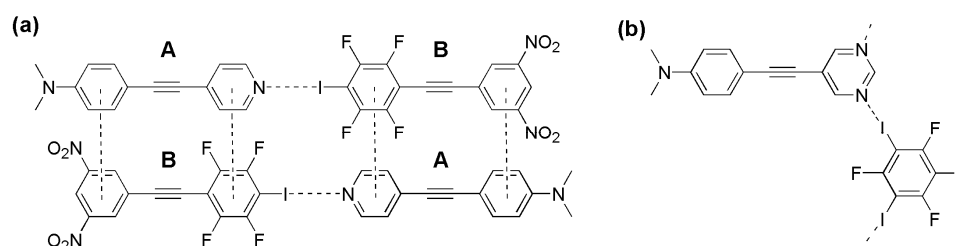


Figure 1. (a) Cooperative halogen bonding and EDA π -stacking in cocrystal **A•B** [12]. (b) Ditopic halogen bonding in cocrystals formed between 5-(*N,N*-dimethylaminophenylethynyl)pyrimidine and 1,3-diiidotetrafluorobenzene [13].

In this manuscript we incorporate ditopic halogen bonding of pyrimidines and π - π stacking. In particular we reasoned that *N,N*-dimethylaminophenylethynyl substituted pyrimidines **1** and **2** as both ditopic halogen bond acceptors and electron rich aromatics for EDA π -stacking when coupled with ditopic halogen bond donor 1-(3,5-dinitrophenylethynyl)-2,4,6-trifluoro-3,5-diiodobenzene, **3** (Figure 2) would form colored cocrystals.

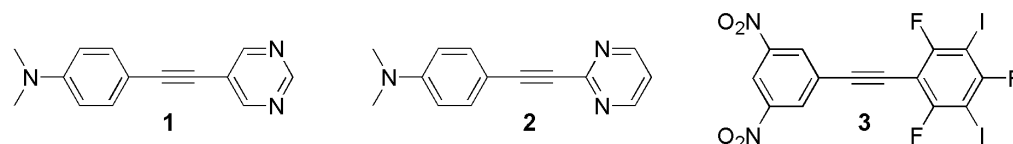


Figure 2. Compounds used in this study.

X-ray crystallography confirms the 3-dimensional arrangement of molecules within each of the cocrystals [**1•3**] and [**2•3**]. Indeed 1:1 cocrystals formed from separate equimolar solutions of the halogen bond donor **3** and each of the pyrimidines **1** and **2** feature 2 unique halogen bonds. They do, however, differ in the π -stacking arrangement within the crystals. Hirschfeld surface analysis using Crystal Explorer 17.5 [14] was used to evaluate close intermolecular contacts within the crystals as well as interaction energies between molecules within the crystalline structure. The relative strengths of individual halogen bonds and π -stacking interactions were calculated using the Gaussian16 software program (Wallingford, CT, USA) [15]. These calculations clearly show that EDA π -stacking is consistently stronger in these cocrystals than halogen bonding. Furthermore, separate calculation of the strengths of halogen bonding and π -stacking in the presence or absence of each other clearly demonstrate both the cooperative effect of halogen bonding on π -stacking and of π -stacking on halogen bonding.

2. Results

2.1. Materials

The compounds **1** and **2** were available from our previous study [13]. Sonogashira coupling of 1-iodo-3,5-dinitrobenzene with trimethylsilylacetylene followed by base deprotection yielded 3,5-dinitrophenylacetylene [12]. 3,5-Dinitrophenylacetylene was reacted

with a 3-fold excess of 1,3,5-trifluoro-2,4,6-triiodobenzene to form the diiodo dinitrotolane (**3**) in 28 % yield shown in Figure 3.

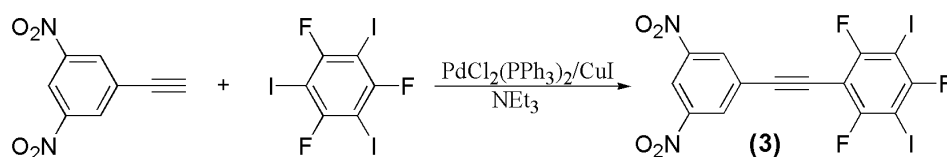


Figure 3. Synthesis of diiodotolane (**3**).

The individual structures of the compounds **1** and **2** used in this study were confirmed by single crystal X-ray analysis and are included in the Supplementary Material.

2.2. Formation and Analysis of Cocrystals

Based on our expectation that the electron-rich pyrimidines **1** and **2** would each form 1:1 cocrystals with diiododinitrotolane **3** we dissolved the pairs of compounds in a 1:1 molar ratio in dichloromethane and allowed slow evaporation of the solvent. In each case the solutions become dark yellow brown as the volume of solvent decreased and ultimately bright red cocrystals formed.

The cocrystal **1•3** crystallized in the triclinic space group P-1. The asymmetric unit contains one molecule of each component as shown in Figure 4. There are two unique halogen bonds with distances I1...N1 and I2#1...N2 of 2.934(3) and 2.978(3) respectively and near linear angles C16-I1...N1 and C18-I2...N2#1 of 176.74(12) and 179.04(13)° respectively.

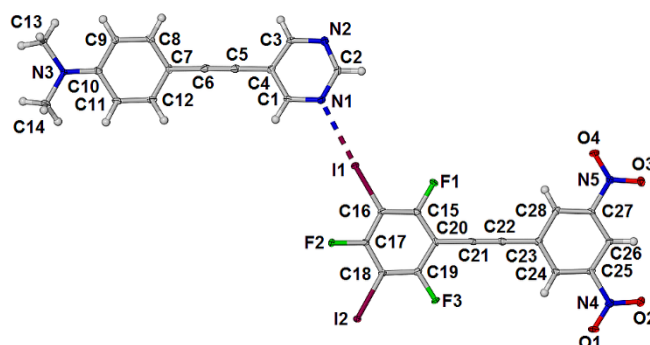


Figure 4. Asymmetric unit of the cocrystal **1•3** with displacement ellipsoids drawn at the 50% level.

The Hirshfeld surface was generated for each of the components and two complementary views are shown in Figure 5 and these surface plots confirm that the halogen bond is the most prominent close contact. These plots also reveal two bifurcated non-conventional C-H...O contacts to each nitro group [16]. Thus, for nitro group O1N4O2 the H8...O1 and H3...O2 distances are 2.59 and 2.58 Å with C8-H8...O1 and C3-H3...O2 angles of 147.0 and 165.7° respectively (see Figure 6). For nitro group O3N5O4 the H1...O3 and H12...O4 distances are 2.55 and 2.58 Å with C12-H12...O4 and C1-H1...O3 angles of 149.0 and 159.5° respectively. In addition to these interactions within the plane of each molecule several less prominent close contacts resulting from π -stacking are visible on the Hirshfeld surface of each molecule.

Each of the two components, **1** and **3**, are essentially planar with an interplanar angle of 12.2(2)° between the planes of the pyridyl and dimethylaminophenyl rings and an interplanar angle of 5.9(3)° between the dinitrophenyl and perhalophenyl rings. Furthermore the interplanar angle across the halogen bond is 12.0(2)°. The halogen bonded interactions along with the cooperative C-H...O interactions result in the formation of one-dimensional zig-zag supramolecular polymers that interdigitate to form an essentially planar 2-dimensional sheet shown in Figure 6.

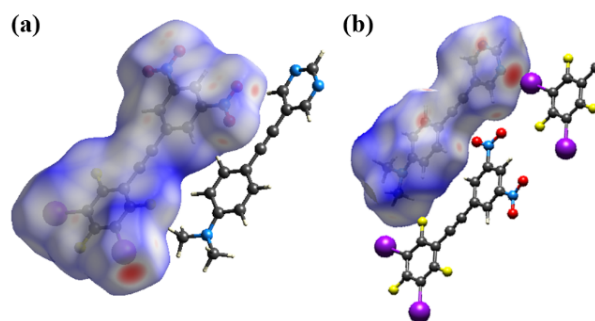


Figure 5. Hirschfeld surface showing d_{norm} for **3** in (a) and for **1** in (b) highlighting the close contacts, in red, between adjacent molecules within the cocrystal **1•3**.

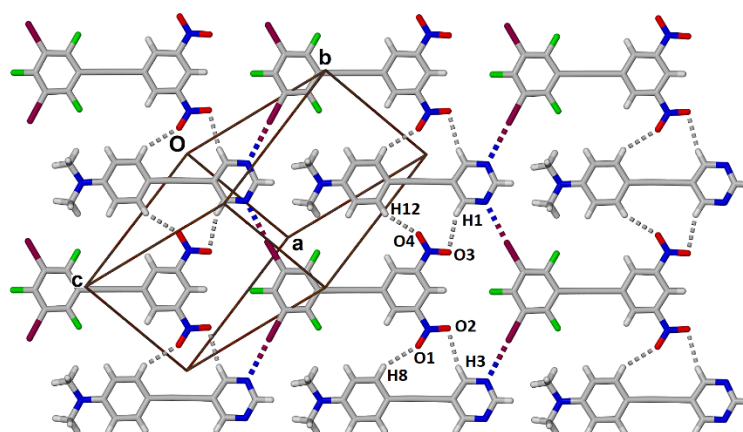


Figure 6. View of the planar sheet formed within the cocrystal **1•3** with halogen bonds shown as colored dashed lines and nonconventional hydrogen bonds shown as grey dashed lines.

The packing of the planar sheets is such that there are three unique offset π -stacking interactions. The expected π -stacked pair **1** and **3** is sandwiched between two offset head-to-tail π -dimers, **1-1** and **3-3** as shown in Figure 7. The π -stacked EDA complex, D-A in Figure 7, is sideways offset as evidenced by the dimethylamino-N atom being above one of the nitro nitrogen atoms with an N-N distance of 3.039(5) Å while H3 of the pyrimidine ring is located 3.17 Å above the centroid of the halogenated benzene. These interactions are labelled “U” and “V” in Figure 7. In contrast the **1-1** and **3-3** π -dimers are offset along the long axis of each molecule. Thus, two molecules of **1** are head-to-tail π -stacked with C2 of one molecule 3.162(6) Å above C7 of the second molecule, shown as “W” in Figure 7. In the π -stacking between two molecules of **3**, also stacked head-to-tail, C17 in the halogenated benzene of one molecule is 3.328(5) Å above C23 in the dinitrobenzene ring of the second molecule, “X” in Figure 7. Each of the interactions U to X are visible as red close contacts on the Hirschfeld surfaces shown in Figure 5.

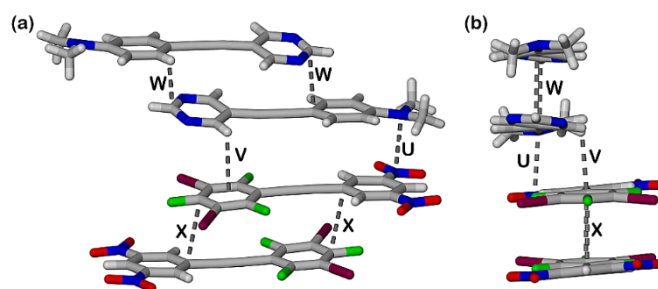


Figure 7. (a) Oblique view of the three unique stacking interactions **1-1**, **1-3** and **3-3** in the cocrystal **1•3** and view along the long axis of the four molecules in (b). Interactions U-X defined in the text.

To investigate the strength of the different π -stacking interactions present (1-1, 1-3 and 3-3), interaction energies were calculated at the B3LYP/DGDZVP level of theory using Crystal Explorer 17.5. Crystal Explorer calculates the total interaction energies (E_{total}) as a sum of electrostatic (E_{ele}), polarization (E_{pol}), dispersion (E_{dis}) and exchange-repulsions terms (E_{rep}). These calculations showed that the 3-3 π -dimer has the largest interaction energy, while the 1-1 π -dimer has the weakest, as seen in Figure 8. In all cases, the π -stacking interactions are driven mainly by dispersion and electrostatic interactions as shown in Table 1, with stacking interactions involving the large iodine atom having higher interaction energies due to large dispersion and electrostatic contributions.

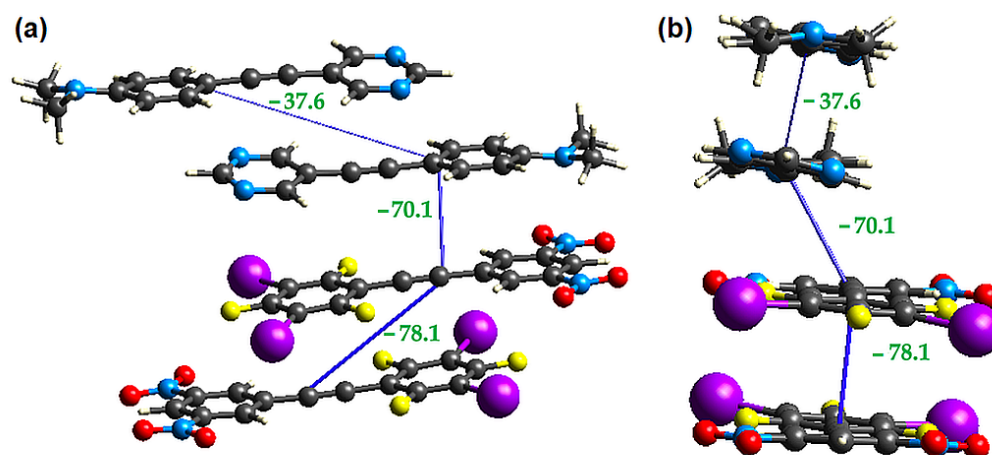


Figure 8. (a) Oblique view of the three unique stacking interactions 1-1, 1-3 and 3-3 in the cocrystal **1•3** and view along the long axis of the four molecules in (b). Interactions' energies (in kJ/mol) are in green.

Table 1. Interaction energies (in kJ/mol) for the unique stacking interactions in the the cocrystal **1•3**.

π -Dimer	E_{ele}	E_{pol}	E_{dis}	E_{rep}	E_{total}
D-D	−53.0	−3.4	−109.9	123.3	−78.1
D-A	−48.9	−4.8	−88.3	100.6	−70.1
A-A	−34.7	−2.3	−59.0	84.4	−37.6

We also examined the strength of the halogen bonds and non-conventional hydrogen bonds that occur between donor and acceptor molecules within the same plane of the cocrystal (Figure 9). These calculations show that the two halogen bonds are equivalent in strength, although examination of the individual components of the interaction energy shows some subtle differences in the individual components (Table 2) likely due to small differences in the intermolecular distances. The two side-by-side 1-3 interactions are quite similar in strength; however, we again observe some differences due to slightly different intermolecular distances between the two interacting species.

The asymmetric unit of the cocrystal formed between **2** and **3** also included one molecule of each of the components as shown in Figure 10. Each of the component molecules **2** and **3** are essentially planar with interplanar angles of 5.84(14) and 8.08(12) $^{\circ}$ respectively between the aromatic rings in molecule **2** and **3**. A major difference to the **1•3** cocrystal is that the molecules do not form a planar sheet. Indeed the second diiododifluorophenyl ring has an interplanar angle of 46.92(7) $^{\circ}$ to the pyrimidine ring and C15#1 is 3.750(10) Å out of the plane defined by the pyrimidine ring (Figure 10).

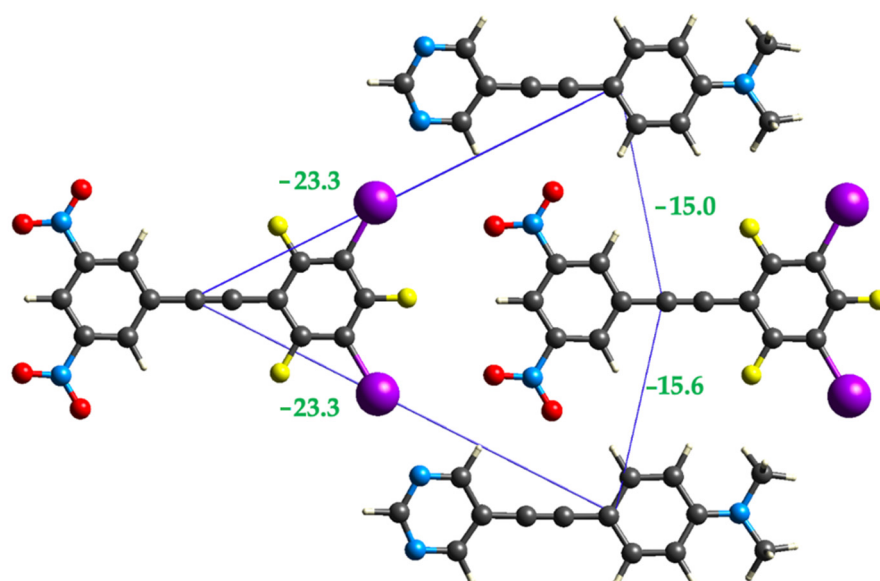


Figure 9. Crystal Explorer interaction energies (in kJ/mol) for halogen bonds and side-by-side interactions between halogen bond donor and acceptor.

Table 2. Intermolecular distances (in Å) and interaction energies (in kJ/mol) for the halogen bonded molecules and the D-A side-by-side interactions in cocrystal **1•3**.

Interaction Type	R ¹	E _{ele}	E _{pol}	E _{dis}	E _{rep}	E _{total}
Halogen bond	12.21	−46.8	−5.6	−9.5	62.5	−23.3
Halogen bond	12.25	−42.3	−5.1	−9.3	53.9	−23.3
Side-by-side	8.41	−13.3	−2.5	−27.2	39.8	−15.0
Side-by-side	8.44	−11.5	−2.5	−26.0	34.0	−15.6

¹ R is the distance between the molecular centroids.

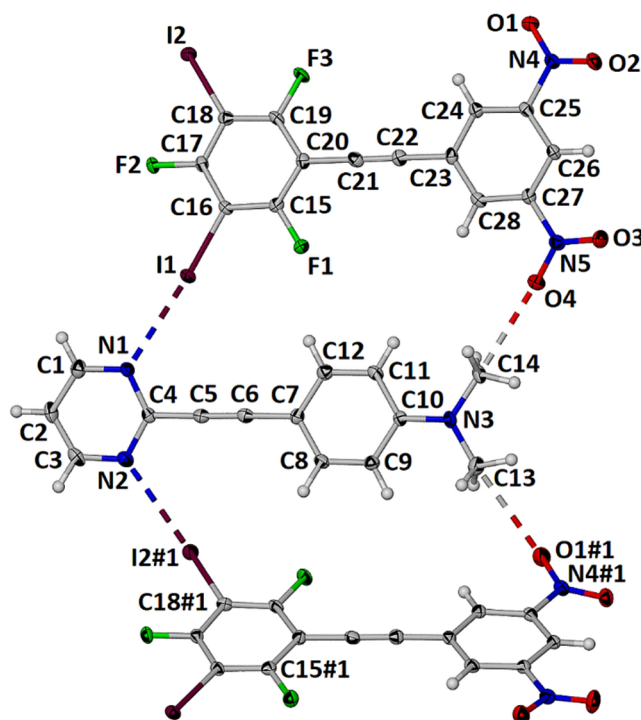


Figure 10. Asymmetric unit of the cocrystal **2•3** with displacement ellipsoids drawn at the 50% level. Halogen bonds and tetrel bonds shown as dashed lines.

There are two unique halogen bonds with distances $I1 \cdots N1$ and $I2\#1 \cdots N2$ of 3.022(3) and 3.261(3) respectively and angles $C16-I1-N1$ and $C18\#1-I2\#1-N2$ of 171.77(9) and 162.93(10)° respectively. These distances, while longer than those in the structure of **1•3**, are 86 and 92% of the sum of the van der Waals radii [17]. It is noteworthy that there are close interactions between nitro O atoms and the amino methyl C atoms. These interactions are reasonably described as tetrel interactions to C [18]. The $C14 \cdots O4$ and $C13\#1 \cdots O3$ separations are 2.905(3) and 3.044(4) Å and the $O4-C14-N3$ and $O1-C13\#1-N3\#1$ angles are 177.5(2) and 165.5(2)° respectively. The $C \cdots O$ separations are 89 and 94% of the sum of the van der Waals radii. These results are in accord with the statistical analysis of tetrel interactions between O and sp^3 -C bonded to N where more linear O-C-N angles correlated to shorter $C \cdots O$ separations [19].

The Hirshfeld surfaces for each molecule shown in Figure 11 highlight these two major close contacts. Along with these two interactions there is a close C-H \cdots F contact with a $H2 \cdots F2$ distance of 2.40 Å (92% the sum of the van der Waals radii). C-H \cdots F interactions are often observed in the structures of fluorinated benzenes [20].

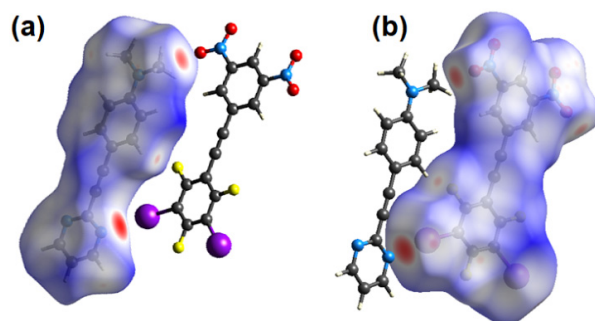


Figure 11. Hirshfeld surface showing d_{norm} for **2** in (a) and for **3** in (b) highlighting the close contacts, in red, between adjacent molecules within the cocrystal **2•3**.

In contrast to the structure **1•3** the one-dimensional ribbons of halogen bonded molecules in **2•3** are alternately corrugated as shown in Figure 12.

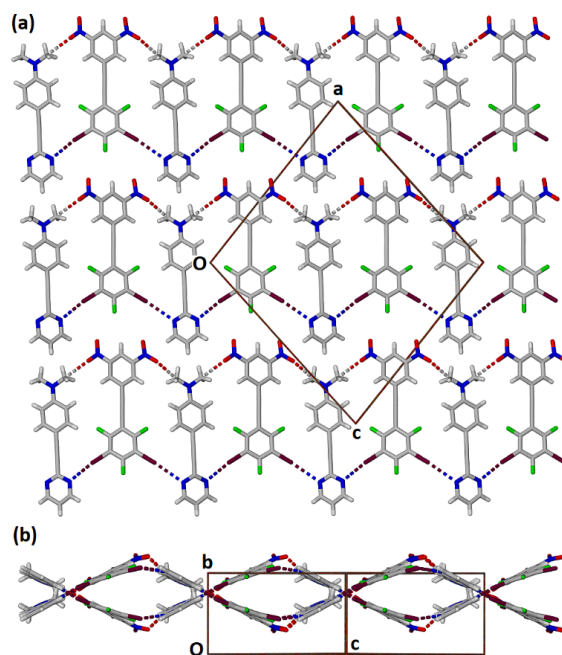


Figure 12. Two views of adjacent alternately corrugated halogen bonded ribbons in the cocrystal **2•3** with halogen bonds and tetrel bonds shown as dashed lines. (a) View along the b axis and (b) view along the line $1\ 0\ -1$.

In contrast to the complex π -stacking observed in **1**•**3**, the molecules within the cocrystal **2**•**3** do stack in alternate of **2** and **3**. However, the stacking is alternately offset along the short axis of each molecule as shown in Figure 13. The face-to-face **2**-**3** orientation, F-F in Figure 13, is also different with the pyrimidine ring and the dinitrophenyl ring stacked rather than the expected stacking of the *N,N*-dimethylaminophenyl ring stacked with the dinitrophenyl ring as in cocrystal **1**•**3**. Thus, in the face-to-face π -interaction the centroid of the dinitrophenyl lies almost directly above the ipso carbon on the pyrimidine ring. The second, offset, π -stacking interaction, O-F-F in Figure 13, has the dimethylamino N atom aligned with one of the iodine atoms on the diiodotrifluorophenyl ring.

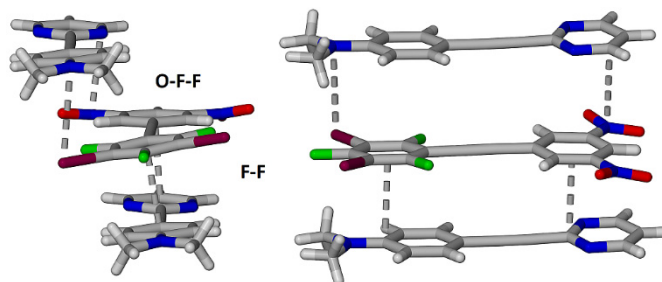


Figure 13. Complementary views of the two unique π -stacking interactions between three adjacent molecules within the cocrystal **2**•**3**.

Crystal Explorer calculations examining the interaction energies for the two π -stacked dimers show that the offset interaction is weaker than the face-to-face interaction (Figure 14) due to a significant decrease in both the electrostatic and dispersion contributions (Table 3).

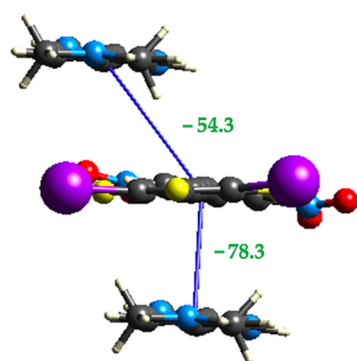


Figure 14. Crystal Explorer interaction energies (in kJ/mol) for the two π -stacking interactions within the cocrystal **2**•**3**.

Table 3. Interaction energies (in kJ/mol) for the unique stacking interactions in cocrystal **2**•**3**.

π -Dimer	E_{ele}	E_{pol}	E_{dis}	E_{rep}	E_{total}
O-F-F	−35.5	−5.2	−72.9	81.9	−54.3
F-F	−54.7	−6.5	−96.7	110.0	−78.4

As expected, calculations on the two halogen bonds show that the halogen bond strength decreases as the halogen bond length increases and the C-I-N angle deviates farther from 180 (Figure 15). Because the halogen bonding and side-by-side interactions in **1**•**3** stem from different partners, these can be considered separately (Table 2). In **2**•**3**, however, the side-by-side nature of the halogen bonding partners precludes similar treatment. In effect, the side-by-side E_{totals} for **2**•**3** encompass both the halogen bonding and the tetral bonding that is absent in **1**•**3** (Table 4). Consequently, the interaction energies between halogen bonded molecules in the cocrystal **2**•**3** are significantly higher than those in cocrystal **1**•**3**. This is likely due to the added contribution of the tetral bond in cocrystal **2**•**3**.

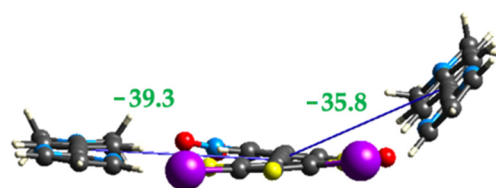


Figure 15. Crystal Explorer interaction energies (in kJ/mol) for the two halogen bonding interactions within cocrystal **2•3**.

Table 4. C-I-N angles and interaction energies (in kJ/mol) between halogen bonded molecules in cocrystal **2•3**.

r_{XB} (Å)	C-I-N Angle (Degrees)	r_{TB} (Å)	E_{ele}	E_{pol}	E_{dis}	E_{rep}	E_{total}
3.022(3)	171.77(9)	2.905(3)	−49.9	−7.5	−27.3	69.4	−39.3
3.261(3)	162.93(10)	3.044(4)	−34.3	−5.3	−31.4	51.3	−35.8

2.3. Computational Analysis of the Interplay between Halogen Bonding and π -Stacking

To evaluate the interplay between halogen bonding and π -stacking and whether the interactions show any cooperativity, trimers that featured a monomer involved in both halogen bonding and π -stacking were taken from the crystal structure and subjected to electronic structure calculations. For each trimer, the strength of the interactions was calculated within the trimer, and as an isolated dimer, and compared. For cocrystal **1•3** this is complicated since there are three unique π -stacking interactions that are treated separately.

Figure 16 shows that when a halogen bond donor in the **1•3** cocrystal is involved in both an electron donor-acceptor π -interaction and a halogen bond there is no significant cooperativity or competition between the two. While small differences in energy are noted, they are possibly due to inaccuracies in the computational methods rather than any true cooperativity/competition. Calculations (results not shown) in which the halogen bond acceptor of the **1-3** π -dimer is making a halogen bond give the same result.

Figures 17 and 18 show the interplay between the **1-1** π -interaction and the halogen bond and the **3-3** π -interaction and the halogen bond, respectively. In both cases we see that the strength of these interactions increases by ~ 2 kcal/mol in the presence of one another, indicating that the two are mutually cooperative.

A similar analysis was carried out on the **2•3** cocrystal. Figures 19 and 20 suggest that there may be weak cooperativity between the face-to-face π -stacking interaction and the halogen bonds since in both cases the strength of both interactions increase slightly in the trimer, relative to the isolated dimers. The magnitude of the difference (~ 0.6 kcal/mol) is like previous work [21,22] and may indicate weak cooperativity, however, the difference is small enough that the evidence is not conclusive.

Analysis of the interplay between the offset **2-3** π -stacking interaction and the bent halogen bond shows a similar result to that of the face-to-face **2-3** π -stacking (Figure 21). When considering the interplay between the offset π -stacking interaction and the linear halogen bond, however, the analysis is complicated by the presence of a non-negligible interaction between the two acceptors (Figure 22). However, if we compare the strength of the π -stacking interaction in the trimer (-20.93 kcal/mol) to the sum of the energies for the two π -stacking dimers (-20.57 kcal/mol) we see that they are very close, indicating no cooperativity. Similarly, if we compare the halogen bond energy in the trimer (-16.87 kcal/mol) to the sum of the energy to break the halogen bond and the stacking interaction in the isolated dimers (-16.57 kcal/mol) we again see that the values are quite close indicating that there is little to no cooperativity.

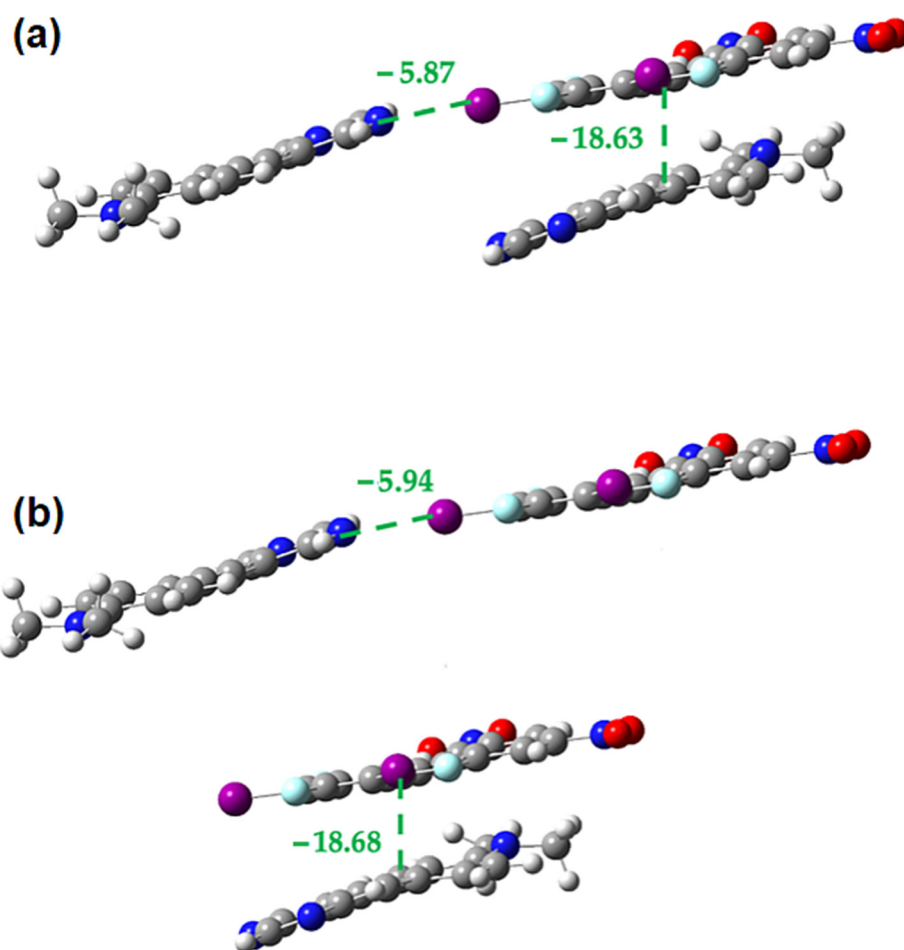


Figure 16. M062X-D3/DGDZVP interaction energies (in kcal/mol) in the **1•3** cocrystal for the interplay between 1-3 π -stacking and halogen bonding (a) within trimer (b) in the isolated dimers.

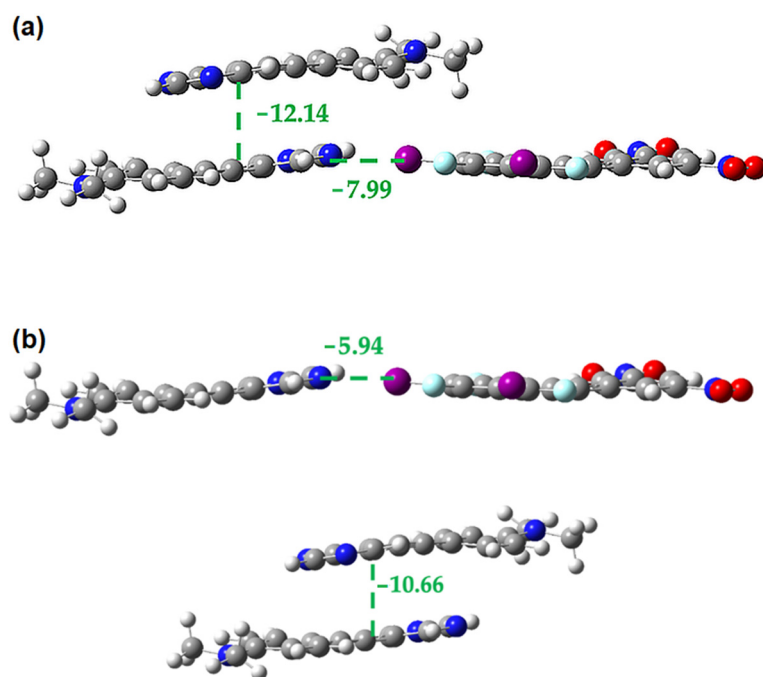


Figure 17. M062X-D3/DGDZVP interaction energies (in kcal/mol) in the **1•3** cocrystal for the interplay between 1-1 π -stacking and halogen bonding (a) within trimer (b) in the isolated dimers.

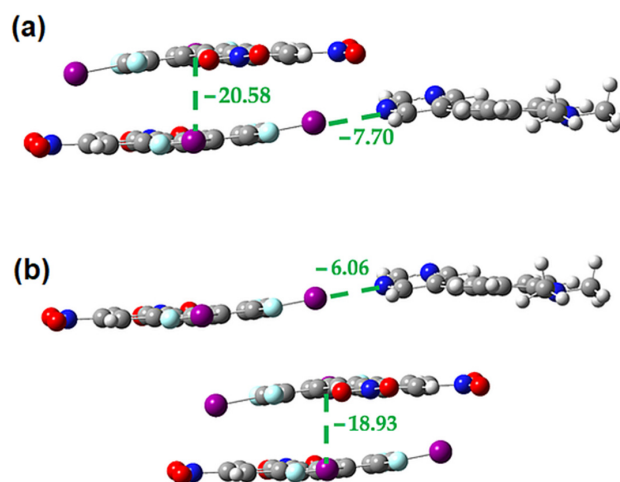


Figure 18. M062X-D3/DGDZVP interaction energies (in kcal/mol) in the **1•3** cocrystal for the interplay between 3-3 π -stacking and halogen bonding (a) within trimer (b) in the isolated dimers.

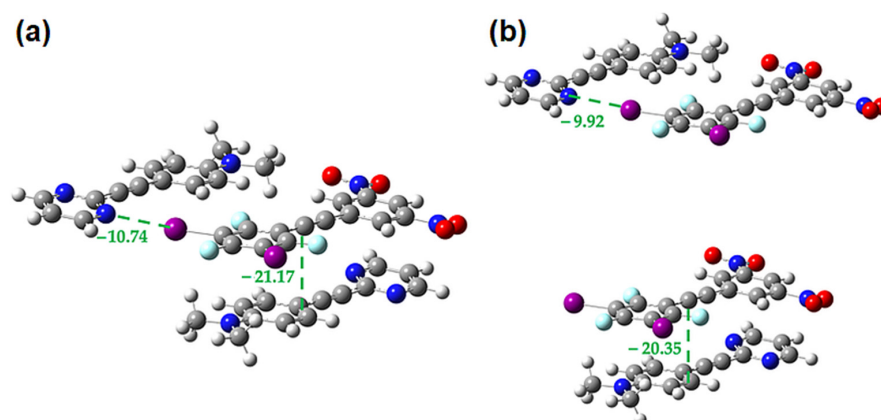


Figure 19. M062X-D3/DGDZVP interaction energies (in kcal/mol) in the **2•3** cocrystal for the interplay between the face-to-face 2-3 π -stacking and the linear halogen bond (a) within trimer (b) in the isolated dimers.

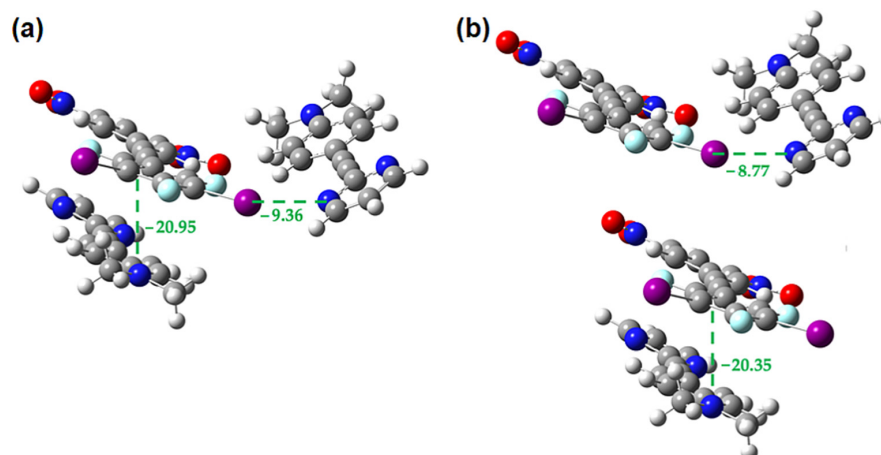


Figure 20. M062X-D3/DGDZVP interaction energies (in kcal/mol) in the **2•3** cocrystal for the interplay between the face-to-face 2-3 π -stacking and the bent halogen bond (a) within trimer (b) in the isolated dimers.

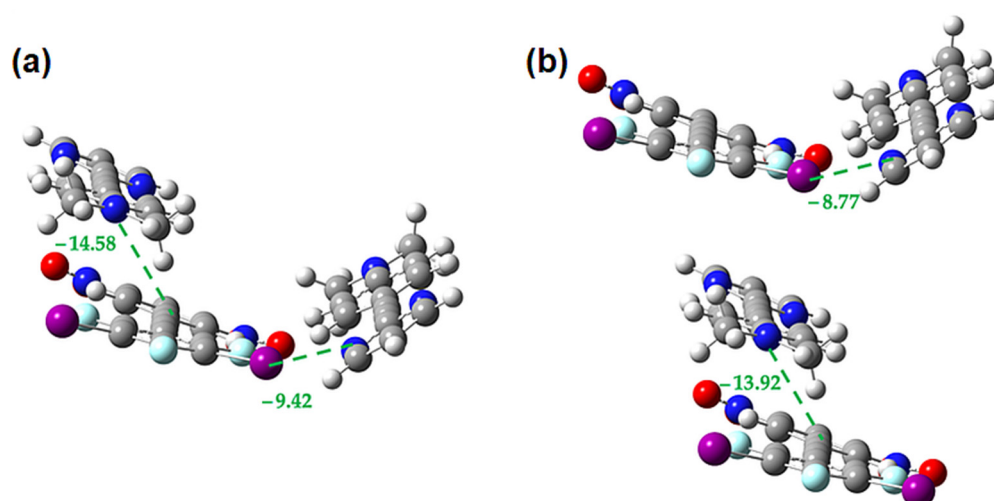


Figure 21. M062X-D3/DGDZVP interaction energies (in kcal/mol) in the **2•3** cocrystal for the interplay between the offset 2-3 π -stacking and the bent halogen bond (a) within trimer (b) in the isolated dimers.

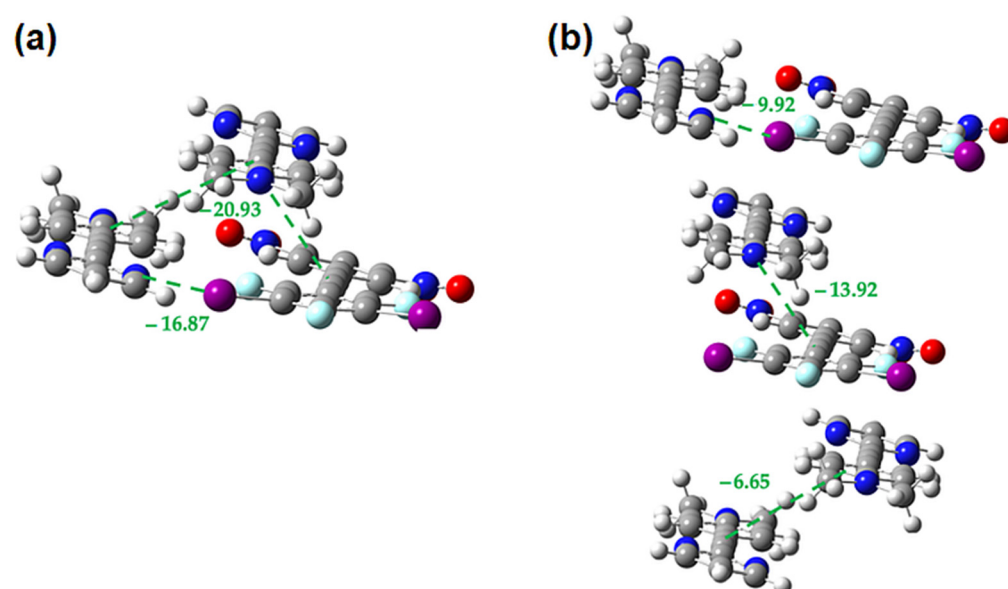


Figure 22. M062X-D3/DGDZVP interaction energies (in kcal/mol) in the **2•3** cocrystal for the interplay between the offset 2-3 π -stacking and the linear halogen bond (a) within trimer (b) in the isolated dimers.

3. Materials and Methods

3.1. Preparation of Materials

Compounds **1** and **2** were available from a previous study [11]. The single crystal X-ray structure of **1** is included in the supporting information. The structure of **2** has been published [23,24]. Compound **3** was prepared through Sonogashira coupling of the corresponding iodoarene and terminal alkyne as shown in Figure 3.

Synthesis of 1,3,5-Trifluoro-2,4-diiodo-(3,5-dinitrophenylethynyl)benzene, **3**. 1-Ethynyl-3,5-dinitrobenzene (0.353 g, 1.83 mmol) and 1,3,5-trifluoro-2,4,6-triodobenzene (2.763 g, 5.42 mmol) were dissolved in a mixture of triethylamine (2 mL) and tetrahydrofuran (5 mL) and argon bubbled through the mixture for 5 min. Bis(triphenylphosphine) palladium(II) chloride (0.035 g) and copper iodide (0.017 g) were added and the reaction mixture was heated at 45 °C for 12 h under an argon atmosphere. The reaction was cooled to room temperature and solvent removed in vacuo. The crude product was di-

luted with dichloromethane and washed with water, followed by brine. After evaporation of the solvent, the crude material was dry loaded onto a silica column and purified by flash column chromatography. Hexanes was run first to recover unreacted 1,3,5-trifluoro-2,4,6-triodobenzene and then the column eluted with increasingly polar mixtures of hexanes/EtOAc until the title compound eluted with 15:1 hexanes:ethyl acetate mixture as colourless crystals (0.285 g, 27%. ^1H NMR (400 MHz): δ 9.08 (1H, t, J 2.3 Hz), 8.73 (2H, d, J 2.3 Hz). ^{19}F NMR (400 MHz): δ -84.1 (d, J 4.0 Hz, 2F), -64.3 (t, J 4.0 Hz, 1F).

3.2. Cocrystallization

5-(4-*N,N*-dimethylaminophenylethynyl)pyrimidine, **1**, (2.6 mg, 0.013 mmol) and 1,3,5-trifluoro-2,4-diiodo-(3,5-dinitrophenylethynyl)benzene, **3** (7.4 mg, 0.013 mmol) were weighed into a screw cap vial. Dichloromethane (2 mL) was added and the mixture vortexed until a homogeneous solution was obtained. The solvent was allowed to slowly evaporate until homogeneous mass of clear red cocrystals, **1•3**, formed. Cocrystal **2•3** was formed following a similar procedure.

3.3. Structure Refinement

Crystal data, data collection and structure refinement details for cocrystals **1•3**, **2•3** and pyrimidines **1** and **2** are summarized in Table S1. Single crystals of each were mounted on a Kryoloop using viscous hydrocarbon oil. Data were collected at 100 K using a Bruker Apex1 CCD diffractometer equipped with Mo $K\alpha$ radiation with $\lambda = 0.71073$ Å. Low temperature data collection was facilitated by use of a Kryoflex system with an accuracy of ± 1 K. Initial data processing was carried out using the Apex 2 software suite (Madison, WI, USA) [25]. Structures were solved by direct methods using SHELXT-2018 [26] and refined against F2 using SHELXL-2018 [27]. The program X-Seed was used as a graphical interface [28]. The aromatic H atoms, all observed in the difference maps, were treated as riding atoms in geometrically idealized positions with C—H = 0.95 (aromatic) or 0.98 Å (methyl) and Uiso (H) = kUeq (C).

3.4. Computational Methods

Interaction energies for the crystal were calculated using Crystal Explorer 17.5 [14,29] at the B3LYP/DGDZVP level of theory [30–33]. The cooperativity and competition between the different intermolecular interactions was explored by carrying out single point energy calculations on the relevant clusters from the crystal structure using the Gaussian16 (rev B.01) software program [15]. All energy calculations were carried out using the M062X-D3 level of theory [34,35] with the DGDZVP basis set [32,33], as used in previous work [12]. All interaction energies were calculated relative to the unrelaxed monomers and were counterpoise corrected [36,37] for basis set superposition error.

4. Conclusions

In conclusion, this combined experimental and computational study demonstrates successful application of cooperative ditopic halogen bonding and electron donor-acceptor π -stacking to the formation of highly colored cocrystals. Importantly, the halogen bonding and π -stacking are both complementary and cooperative.

Supplementary Materials: The following are available online, Table S1, Table S2 and Figure S1: Crystallographic data.

Author Contributions: Conceptualization, E.B.; Data curation, E.D.S. and E.B.; Formal analysis, E.D.S., C.I.N. and E.B.; Funding acquisition, E.D.S., N.P.B. and E.B.; Investigation, E.D.S., C.I.N. and E.B.; Methodology, E.D.S. and E.B.; Project administration, E.B.; Resources, E.D.S. and E.B.; Software, E.D.S. and E.B.; Supervision, E.D.S. and E.B.; Validation, E.D.S., N.P.B. and E.B.; Visualization, E.B.; Writing—original draft, E.D.S. and E.B.; Writing—review & editing, E.D.S., C.I.N., N.P.B. and E.B. All authors have read and agreed to the published version of the manuscript.

Funding: This research was funded by the National Science Foundation (RUI Grant Nos. CHE1606556 and CHE1903581) and the Missouri State University Provost Incentive Fund, which funded the purchase of the X-ray diffractometer. Computational resources were provided by NSF-MRI awards CHE1039925 and OAC1919571 through the Midwest Undergraduate Computational Chemistry Consortium—MU3C.

Institutional Review Board Statement: Not applicable.

Informed Consent Statement: Not applicable.

Data Availability Statement: Crystallographic data has been deposited with the CCDC.

Conflicts of Interest: The authors declare no conflict of interest.

Sample Availability: Samples of the compounds are not available from the authors.

References

1. Rest, C.; Kandanelli, R.; Fernandez, G. Strategies to create hierarchical self-assembled structures via cooperative non-covalent interactions. *Chem. Soc. Rev.* **2015**, *44*, 2543–2572. [[CrossRef](#)] [[PubMed](#)]
2. Saha, S.; Sastry, G.N. Cooperative or Anticooperative: How Noncovalent Interactions Influence Each Other. *J. Phys. Chem. B* **2015**, *119*, 11121–11135. [[CrossRef](#)] [[PubMed](#)]
3. Dong, R.; Zhou, Y.; Zhu, X. Supramolecular Dendritic Polymers: From Synthesis to Applications. *Acc. Chem. Res.* **2014**, *47*, 2006–2016. [[PubMed](#)]
4. Li, F.; Yager, K.G.; Dawson, N.M.; Jiang, Y.-B.; Malloy, K.J.; Qin, Y. Stable and Controllable Polymer/Fullerene Composite Nanofibers through Cooperative Noncovalent Interactions for Organic Photovoltaics. *Chem. Mater.* **2014**, *26*, 3747–3756. [[CrossRef](#)]
5. Huang, Z.; Qin, K.; Deng, G.; Wu, G.; Bai, Y.; Xu, J.; Wang, Z.; Yu, Z.; Scherman, O.A.; Zhang, X. Supramolecular Chemistry of Cucurbiturils: Tuning Cooperativity with Multiple Noncovalent Interactions from Positive to Negative. *Langmuir* **2016**, *32*, 12352–12360. [[CrossRef](#)]
6. Loh, C.C.J. Exploiting non-covalent interactions in selective carbohydrate synthesis. *Nat. Rev. Chem.* **2021**, *5*, 792–815. [[CrossRef](#)]
7. Motloch, P.; Bols, P.S.; Anderson, H.L.; Hunter, C.A. Cooperative assembly of H-bonded rosettes inside a porphyrin nanoring. *Chem. Sci.* **2021**, *12*, 1427–1432. [[CrossRef](#)]
8. Quentin, J.; Swenson, D.C.; MacGillivray, L.R. Supramolecular Sandwiches: Halogen-Bonded Cofomers Direct [2+2] Photoreactivity in Two-Component Cocrystals. *Molecules* **2020**, *25*, 907.
9. Majumdar, P.; Tharammal, F.; Gierschner, J.; Varghese, S. Tuning Solid-State Luminescence in Conjugated Organic Materials: Control of Excitonic and Excimeric Contributions through π Stacking and Halogen Bond Driven Self-Assembly. *ChemPhysChem* **2020**, *21*, 616–624. [[CrossRef](#)]
10. Liu, Y.H.; Dadvand, A.; Titi, H.M.; Hamzehpoor, E.; Perepichka, D.H. Halogen bonding vs. π -stacking interactions in new bis(acenaphthylene)dione semiconductors. *CrystEngComm* **2021**, *23*, 8255–8259. [[CrossRef](#)]
11. Zhu, W.; Zheng, R.; Zhen, Y.; Yu, Z.; Dong, H.; Fu, H.; Shi, Q.; Hu, W. Rational Design of Charge-Transfer Interactions in Halogen-Bonded Co-crystals toward Versatile Solid-State Optoelectronics. *J. Am. Chem. Soc.* **2015**, *137*, 11038–11046. [[CrossRef](#)] [[PubMed](#)]
12. Nwachukwu, C.I.; Kehoe, Z.R.; Bowling, N.P.; Speetzen, E.D.; Bosch, E. Cooperative halogen bonding and polarized π -stacking in the formation of colored mixed-stack charge-transfer co-crystals. *New J. Chem.* **2018**, *42*, 10615–10622. [[CrossRef](#)]
13. Nwachukwu, C.I.; Patton, L.J.; Bowling, N.P.; Bosch, E. Ditopic halogen bonding with bipyrimidines and activated pyrimidines. *Acta Cryst.* **2020**, *C76*, 458–467. [[CrossRef](#)] [[PubMed](#)]
14. Turner, M.J.; McKinnon, J.J.; Wolff, S.K.; Gromwood, D.J.; Spackman, P.R.; Jayatilaka, D.; Spackman, M.A. *Crystal Explorer 17.5*; University of Western Australia: Perth, Australia, 2017.
15. Frisch, M.J.; Trucks, G.W.; Schlegel, H.B.; Scuseria, G.E.; Robb, M.A.; Cheeseman, J.R.; Scalmani, G.; Barone, V.; Petersson, G.A.; Nakatsuji, H.; et al. *Gaussian 16, Revision B.01*; Gaussian, Inc.: Wallingford, CT, USA, 2016.
16. Dey, S.K.; Ojha, B.; Das, G. A subtle interplay of C–H hydrogen bonds in complexation of anions of varied dimensionality by a nitro functionalized tripodal podand. *CrystEngComm* **2011**, *13*, 269–278. [[CrossRef](#)]
17. Bondi, A. van der Waals Volumes and Radii. *J. Phys. Chem.* **1964**, *68*, 441–451. [[CrossRef](#)]
18. Bauza, A.; Mooibroek, T.J.; Frontera, A. Tetrel-Bonding Interaction: Rediscovered Supramolecular Force? *Angew. Chem. Int. Ed.* **2013**, *52*, 12317–12321. [[CrossRef](#)]
19. Veluthaparam, R.V.P.; Saha, A.; Saha, B.K. The Effects of Electronegativity of X and Hybridization of C on the X–C \cdots O Interactions: A Statistical Analysis on Tetrel Bonding. *ChemPlusChem* **2021**, *86*, 1123–1127. [[CrossRef](#)]
20. Thalladi, V.R.; Weiss, H.-C.; Blaser, D.; Boese, R.; Nangia, A.; Desiraju, G.R. C–H \cdots F Interactions in the Crystal Structures of Some Fluorobenzenes. *J. Am. Chem. Soc.* **1998**, *120*, 8702. [[CrossRef](#)]
21. Bowling, N.P.; Speetzen, E.D.; Bosch, E. Arylethynyl Helices Supported by π -Stacking and Halogen Bonding. *ChemPlusChem* **2021**, *86*, 745. [[CrossRef](#)]

22. Zhu, H.Y.; Wu, J.Y.; Dai, G.L. Study on the Halogen Bond and π - π -Stacking Interaction between Fluoro Substituted Iodobenzene and Pyrazine. *J. Mol. Model.* **2020**, *26*, 333. [[CrossRef](#)]
23. Kautny, P.; Kriegner, H.; Bader, D.; Dusek, M.; Reider, G.A.; Frohlich, J.; Stoge, B. Ethyne-Linked Push–Pull Chromophores: Implications of Crystal Structure and Molecular Electronics on the Quadric Nonlinear Activity. *Cryst. Growth Des.* **2017**, *17*, 4124–4136. [[CrossRef](#)]
24. Bosch, E. CCDC 2129575: Experimental Crystal Structure Determination. 2021. Available online: <https://doi.org/10.5517/ccdc.csd.cc29gzzr> (accessed on 14 February 2022).
25. Apex 2; Bruker AXS: Madison, WI, USA, 2014.
26. Sheldrick, G.M. SHELXT—Integrated space-group and crystal-structure determination. *Acta Crystallogr. Sect. A Found. Adv.* **2015**, *A71*, 3–8. [[CrossRef](#)] [[PubMed](#)]
27. Sheldrick, G.M. Crystal structure refinement with SHELXL. *Acta Crystallogr. Sect. C Struct. Chem.* **2015**, *C71*, 3–8. [[CrossRef](#)] [[PubMed](#)]
28. Barbour, L.J. X-Seed—A software tool for supramolecular crystallography. *J. Supramol. Chem.* **2001**, *1*, 189–191. [[CrossRef](#)]
29. Mackenzie, C.F.; Spackman, P.R.; Jayatilaka, D.; Spackman, M.A. CrystalExplorer Model Energies and Energy Frameworks: Extension to Metal Coordination Compounds, Organic Salts, Solvates and Open-Shell Systems. *IUCr* **2017**, *4*, 575–587. [[CrossRef](#)]
30. Becke, A.D. Density Functional Thermochemistry. III. The Role of Exact Exchange. *J. Chem. Phys.* **1993**, *98*, 5642–5648. [[CrossRef](#)]
31. Stephens, P.J.; Devlin, F.J.; Chabalowski, C.F.; Frisch, M.J. Ab Initio Calculation of Vibrational Absorption and Circular Dichroism Spectra Using Density Functional Force Fields. *J. Phys. Chem.* **1994**, *98*, 11623–11627. [[CrossRef](#)]
32. Godbout, N.; Salahub, D.R.; Andzelm, J.; Wimmer, E. Optimization of Gaussian-Type Basis Sets for Local Spin Density Functional Calculations. Part I. Boron through Neon, Optimization Technique and Validation. *Can. J. Chem.* **1992**, *70*, 560–571. [[CrossRef](#)]
33. Sosa, C.; Andzelm, J.; Elkin, B.C.; Wimmer, E.; Dobbs, K.D.; Dixon, D.A. A Local Density Functional Study of the Structure and Vibrational Frequencies of Molecular Transition-Metal Compounds. *J. Phys. Chem.* **1992**, *96*, 6630–6636. [[CrossRef](#)]
34. Zhao, Y.; Truhlar, D.G. The M06 Suite of Density Functionals for Main Group Thermochemistry, Thermochemical Kinetics, Non-Covalent Interactions, Excited States, and Transition Elements: Two New Functionals and Systematic Testing of Four M06-Class Functionals and 12 Other Functionals. *Theor. Chem. Acc.* **2008**, *120*, 215–241.
35. Grimme, S.; Antony, J.; Ehrlich, S.E.; Krieg, J. A Consistent and Accurate Ab Initio Parameterization of Density Functional Dispersion Correction (DFT-D) for the 94 Elements H–Pu. *J. Chem. Phys.* **2010**, *132*, 154104. [[CrossRef](#)] [[PubMed](#)]
36. Boys, S.F.; Bernardi, F. Calculation of Small Molecular Interactions by Differences of Separate Total Energies—Some Procedures with Reduced Errors. *Mol. Phys.* **1970**, *19*, 553–566. [[CrossRef](#)]
37. Simon, S.; Duran, M.; Dannenberg, J.J. How Does Basis Set Superposition Error Change the Potential Surfaces for Hydrogen Bonded Dimers? *J. Chem. Phys.* **1996**, *105*, 11024–11031. [[CrossRef](#)]